ATTENUATION MEASUREMENT AT MICROWAVE FREQUENCIES OF THIN METALLIC FILMS

A Thesis

Presented to

the Faculty of Graduate Studies and Research

The University of Manitoba

In Partial Fulfilment

of the Requirement of the Degree

Master of Science in Electrical Engineering

---

by

Hyung Do Kim

September 1967

ACKNOWLEDGEMENTS

The author wishes to thank Professor Ernest Bridges of the University of Manitoba for suggesting the problem and for his guidance throughout the project.

The author also wishes to express his sincere thanks to the National Research Council and the University of Manitoba Graduate Research Fund for their financial assistance under, respectively, Grants A2702 and 0132364.

ABSTRACT

In this thesis, thin film deposition and thickness measurement techniques are described. The transmission coefficient of a thin metallic film located in the cross-section of a rectangular waveguide operating in the TE_{10} mode is determined analytically and experimentally. Taken into account is the size effect on the conductivity of the thin film. The transmission coefficient measurement at 10 GHz used a microwave bridge and values were obtained for silver films with the thicknesses ranging from 100-1000 Å. Results were in good agreement with those predicted theoretically.

TABLE OF CONTENTS

CHAPTER		PAGE
I	INTRODUCTION	1
II	PREPARATION OF THE THIN FILM	4
	2.1 Vacuum Deposition of a Thin Film ..	4
	Evaporation Source	4
	Residual Gas Effects	6
	2.2 Structure of the Condensed Film ..	7
	2.3 Thin Film Resistivity	8
	2.4 Determination of Film Thickness ..	9
	Weighing Method	9
	Quartz Crystal Microbalance	10
	Calibration of Quartz Crystal Microbalance	13
III	MICROWAVE PROPERTIES OF A THIN METALLIC FILM	14
	3.1 Waves in a Conducting Medium	16
	3.2 Thin Film Transmission, Reflection, and Absorption Coefficients	18
IV	TRANSMISSION COEFFICIENT MEASUREMENT ...	24
	4.1 Thin Film Conductivity Measurement	24
	Four Probe Technique	24
	The Effects Due to the Sample Boundary	26
	4.2 Transmission Coefficient Measurement	30
	Discription of Waveguide Bridge ..	32

CHAPTER		PAGE
	Frequency Stabilization	33
	Film Insertion Device	36
V	DISCUSSION AND SUMMARY OF THE RESULTS ..	40
REFERENCES	....	44

LIST OF FIGURES

FIGURE		PAGE
2.1	Vacuum deposition arrangement	5
2.2	Quartz crystal resonant frequency monitoring device	12
2.3	Calibration curve for quartz crystal microbalance	15
3.1	Rectangular waveguide with metallic film ..	16
3.2	Thin metallic film equivalent circuit	18
3.3	Theoretical transmittance, reflectance, and absorption versus thickness for filver film	22
3.4	Theoretical transmittance, reflectance, and absorption versus film thickness for gold	23
4.1	Four probe arrangement	25
4.2	Image due to the film boundary	26
4.3	Conductivity versus thickness	29
4.4	Microwave bridge	31
4.5	Frequency stabilization of signal source ..	34
4.6	Frequency stabilization of local oscillator	34
4.7	Low pass filter for the local oscillator ..	35
4.8	Film insertion device	37
4.9	Comparison of experimental and theoretical transmission coefficient versus conductivity per square	39

FIGURE		PAGE
5.1	Comparison of experimental and theoretical transmission coefficient versus film thickness for silver	42
5.2	Comparison of experimental and theoretical transmission coefficient versus film thickness for gold	44

CHAPTER I

INTRODUCTION

Although the physics of thin films has a long history, its theoretical basis is still far from being completely established. Often theoretical and experimental results disagree. One particular problem of interest is the transmission of an electromagnetic wave through thin metallic films. It was Kaplan[1] who in 1964 put forward a theoretical formula for the transmission coefficient, T, (the ratio of the transmitted to the incident wave amplitude) taking into account the size effect. Later, in 1964, Korolev and Gridnev[2] performed an experiment to determine this coefficient for silver film of thicknesses of 20-200 Å using a microwave frequency and reported that the values were much less than theoretical ones calculated on the basis of the formula given by Kaplan. No explanations were offered. In 1967 Weck and Lump[3] performed a similar experiment using a coaxial line technique and found no such discrepancies. Kaplan[4] later pointed out there were mistakes in Korolev and Gridnev's experimental results. In reply, Korolev and Gridnev[5] admitted to some of these mistakes, but insisted that these mistakes did not invalidate the reported disagreement between the experimental and theoretical curves. Thus the question is still unsettled.

This investigation is an attempt to settle the question as to whether such a discrepancy does exist by performing a similar experiment. The experiments were performed in two stages in order to check the result more rigorously. First,

the film conductivity, σ, is examined at various thicknesses, d. Secondly, the transmission coefficient is measured against film conductance per square (σd) which can be determined experimentally without knowing the thickness and specific conductivity of a given film.

For a good conducting medium the transmission coefficient is negligibly small at microwave frequencies even when the material thickness is much less than the skin depth; e.g. for silver, the transmission coefficient is less than -40 db when the film thickness is 100 Å which is 1/100 of the skin depth. Such a characteristic is attributed to the high reflection coefficient at the surface due to the impedance mismatch. This property is widely used in microwave mirrors, for shielding purposes, for satellite communication, and in microelectronics.

In chapter II the film forming technique is discussed, as well as the factors affecting the film characteristics. The weighing method used to determine film thickness is described.

In chapter III a theoretical analysis determining the transmission, reflection, and absorption coefficients is given and the size effect on the conductivity of thin metallic films is discussed.

Chapter IV contains a description of the four probe technique used to measure thin film conductivity. The transmission coefficient measurement technique is described, and included

is a desciption of the film insertion device. Precautions taken to ensure frequency stabilization are outlined.

In chapter V the experimental results are discussed and the conclusions given.

CHAPTER II

PREPARATION OF THE THIN FILM

Silver film was primarily used for this investigation and a vacuum deposition technique was used to prepare the films ranging in thickness from 100 Å to 1000 Å. The film was formed on a freshly cleaved mica substrate using a tungsten filament source. The pressure used was 10^{-5} torr and the deposition rate approximately 75 Å per second. The film thickness was measured by a weighing method using a quartz crystal micro-balance.

Some factors which influence the film structure and the thickness monitoring technique are discussed in this chapter.

2.1 Vacuume Deposition of a Thin Film

Evaporation Source

The evaporation source, shown in Figure 2.1, consists of a tungsten filament, a shutter, and an aperture. The filament is a 0.5 mm diameter tungsten wire and the current supplied from a variac controlled transformer. The silver to be evaporated is wetted on the filament to form the evaporation source. Any contaminant must first be driven off from the filament surface by an initial heating. (approximately 2000° C). When the evaporation process is started a shutter is interposed between source and substrate in order to intercept the first portion of the evaporated material which may contain impurities from the molten silver surface.

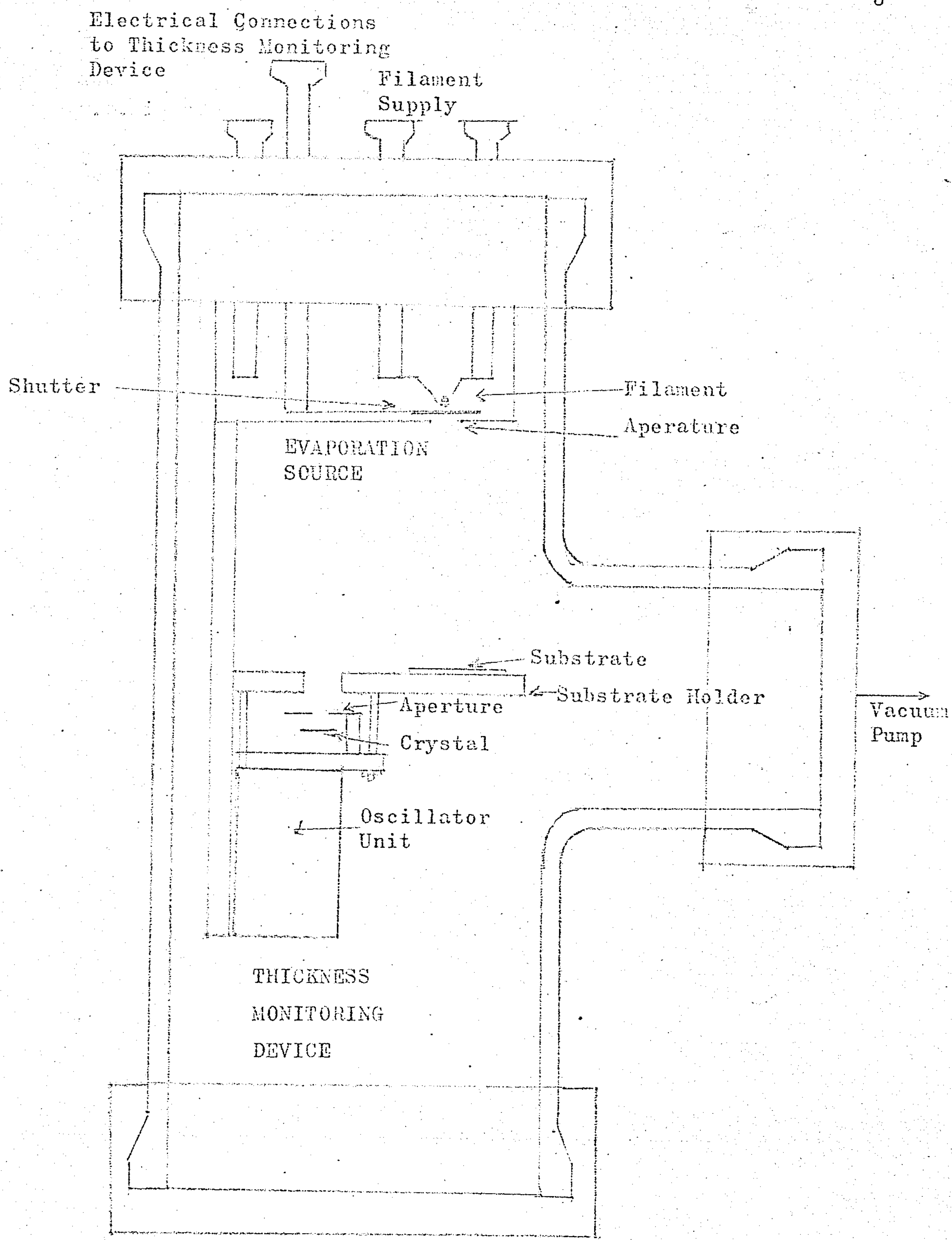

FIG. 2.1

VACUUM DEPOSITION ARRANGEMENT

The degree of contamination of the silver film by the tungsten filament has been determined by Heavens[6] using a radioactive tracer method and it does not exceed a few parts per million under best conditions. These impurities, however, may not affect the resistivity of the metal film at room temperature significantly[7].

Residual Gas Effects

In the deposition of thin films by the evaporation method, it is necessary to maintain a vacuum such that the mean free path of the volatized atoms is large compared to the source to substrate distance. The value of the mean free path of a silver atom is 450 cm when the residual gas is oxygen with pressure of 10^{-5} torr[19]. At this pressure the evaporated atoms make neglegibly few collisions with the residual gas molecules and hence form a molecular beam.

On the basis of kinetic theory of gases the number of molecules, N, striking unit area of a substrate surface in unit time under pressure, P, and absolute temperature, T, is given by

$$N = P/(2\pi mkT)^{\frac{1}{2}}, \qquad (2.1)$$

where k is Boltzmann's constant and m is the mass of a gas molecule. For oxygen at 10^{-5} torr and at room temperature the value of N is sufficient to form a monolayer at the substrate

surface within a few seconds. At this rate of deposition the residual gas layer does not affect the film structure seriously since the binding energy between silver atoms is much larger than those of gas and silver.[8]

2.2 Structure of The Condensed Film

It has been shown by Appleyard[9] that the structure of a thin film deposited onto a solid substrate may be in the form of either a monolayer or an agglomerate of atoms. He states that if the latent heat of evaporation of a metal atom from the surface of the substrate is less than that from the metal itself then an agglomeration is formed due to its lower energy. If the reverse is true then the monolayer form is favored. For a silver film deposited on a mica substrate, the latent heat of evaporation from the metal is approximately seven times higher than that from the substrate surface and hence the film has an agglomerate surface.

The temperature of the substrate is closely related to the structure of the film since it affects the mobility of the deposited atoms. According to a model proposed by Lennard-Jones[10] the surface of the substrate, as a consequence of the lattice structure, can be considered as a series of potential hills and valleys. An atom can move freely on the surface provided that it has a kinetic energy which is greater than the potential difference between the hills and valleys on the surface. Since this kinetic energy is much lower than

that required for evaporation, free motion of the atom occurs on the surface at a temperature far below that needed to evaporate the atom from the surface. As a result, the atom of a high melting point metal has a low mobility whereas that of a low melting point metal has a higher mobility.

If the temperature of the substrate is increased the condensed atoms gain kinetic energy. Their mobility is increased and the structure of the film becomes more agglomerate. On the other hand, if the substrate is maintained at a very low temperature, many defects are frozen into the film structure because the atoms hit the substrate and lose their energy very quickly. This phenomena has been studied by Levinstein [11] using the electron microscope and he found that the silver films prepared by a fast evaporation method were almost continuous when their film thickness reached 100 Å.

2.3 Thin Film Resistivity

It is well known that the resistivity of a thin metal film is higher than that of the bulk form due to the limitation of the mean free path of the conducting electron. A discussion of this effect is given in chapter III. Generally, the experimental value for the resistivity of a thin film is higher than its theoretical value. This discrepancy can be attributed to the granular structure of the film. This granularity can be minimized by employing a fast evaporation technique, 75 Å/sec, and maintaining a low residual gas pressure, 1×10^{-5} torr. The resistivity of films immediately after deposition differs

substantially from the theoretical value. It is necessary to allow a time lapse at room temperature for deposited atoms to arrange themselves into a proper crystal structure. The resistivity was measured 20 minutes after deposition by the four probe technique described in chapter IV. Under these conditions, the measured values of resistivity are quite close to the theoretical values, as is shown in Figure 4.3 for film thicknesses above 100 Å. The theoretical curve is computed from equations presented in chapter IV for the case of diffusive scattering at the film boundaries using a mean free path, Λ_o, of 570 Å. The results are in reasonable agreement with those given by Reynolds and Stilwell[12] as is shown in Figure 4.3.

2.4 Determination of Film Thickness

Weighing Method

Film thickness, d, may be expressed in terms of mass, Δm, deposited in given area, S, thus:

$$d = \Delta m/\rho S, \qquad (2.2)$$

where ρ is the specific gravity of the material to be evaporated. It is, however, difficult to define a thickness for very thin films due to the granular structure at the initial growing stage. In order to determine the range of film thickness which can be relied upon to yield correct results an experiment has been performed by Clegg and Crook[13] using a rapidly

evaporated (75 Å/sec) silver film deposited on a mica substrate. In their experiment the film thickness was first determined with a torsion balance, with a sensitivity of 0.5×10^{-6} gm/cm^2, installed inside a vacuum chamber and then later checked with a Tolansky multiple beam interferomenter[14]. The two independent methods of determining film thickness were in agreement within a few percent for the film thickness down to 120 Å.

The film thickness in our experiment is determined by measuring the mass, Δm, with a quartz crystal microbalance which is described in the following section.

Quartz Crystal Microbalance

The quartz crystal microbalance is arranged as shown in Figure 2.1. When the film is deposited on the substrate some of the film is deposited on the quartz crystal surface through the aperture. The ratio of the mass deposited on the quartz crystal to that on the substrate is a constant since the geometry of the substrate, quartz crystal and the beam source are fixed.

The mass, Δm, deposited on a given area, A, of the quartz crystal is obtained by monitoring the change in its resonant frequency, Δf, during the deposition process. The relation between Δm and Δf is given by Sauerbrey[15] as follow:

$$\Delta m = c\Delta f, \qquad (2.3)$$

where c is the proportionality constant and is given by

$$c = -f_0 / k\rho tA,$$

t is the thickness of the quartz crystal, ρ is the density of the deposited material, f_0 is the resonant frequency of the quartz crystal, and k is a constant approximately equal to unity and depending on the distribution of the mass over the crystal surface. Equation (2.3) shows that the mass deposited on a crystal is linearly proportional to the change in resonant frequency of the quartz crystal, provided that Δf is much less than the resonant frequency f_0.

In order to avoid the temperature effect due to the accumulation of heat from the evaporation source, the AT crystal cut, which possesses a relatively low temperature coefficient, and a heat shield as shown in Figure 2.1 are employed. The experimental results show that the frequency drift due to the temperature effect at 1000 Å is less than a few hertz.

The circuit for monitoring resonant frequency is composed of a conventional Colpit's oscillator and an emitter follower stage to isolate the oscillator from the load, as shown in Figure 2.3. The usual practice is to use a pair of flexible coaxial cables to connect the crystal and an oscillator circuit which is installed outside of the vacuum chamber. The cable capacitance which appears across the crystal may cause a frequency drift due to cable bending in addition to cable noise pickup. In order to overcome this problem the oscillator

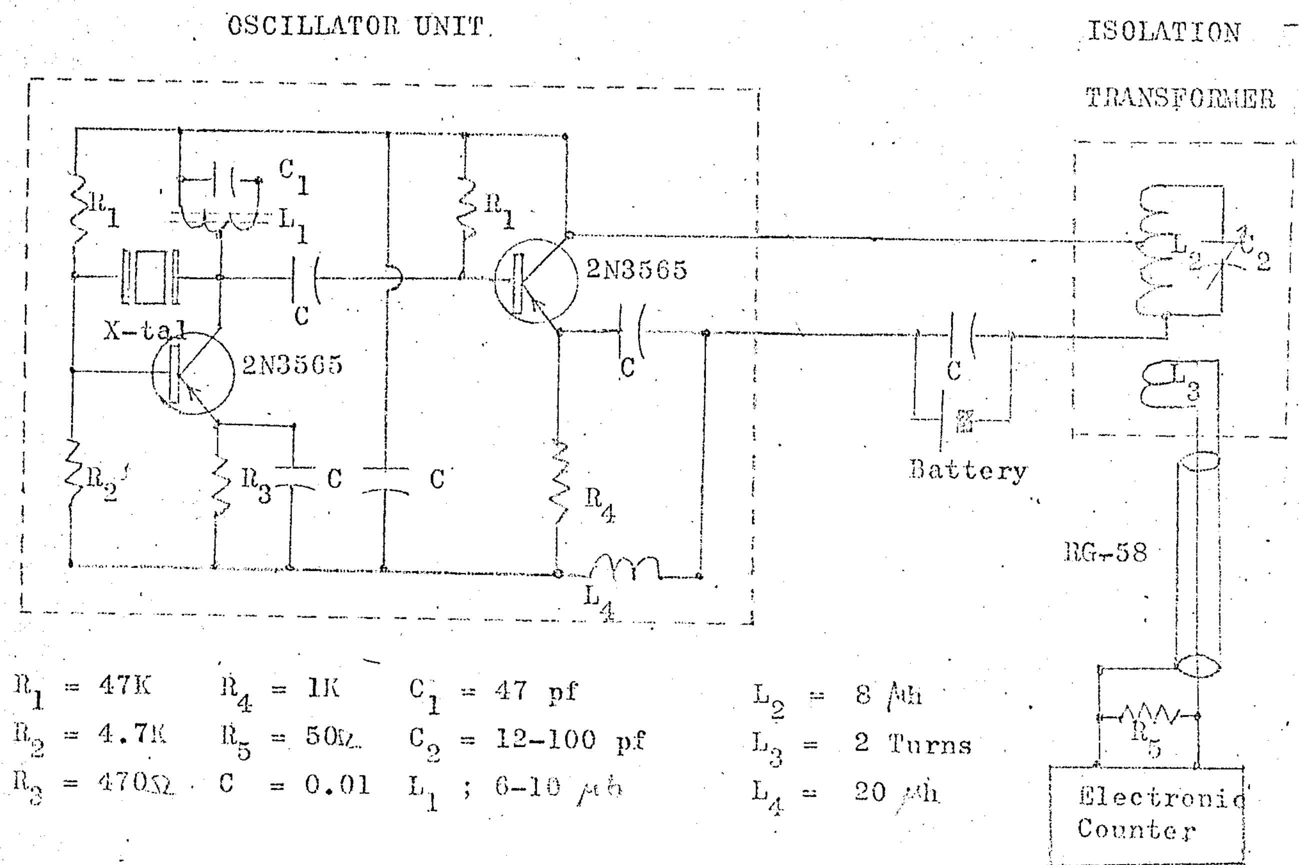

Fig. 2.2 Quartz crystal resonant frequency monitoring device.

circuit was built inside a 2.5 cm diameter by 3 cm high aluminium container and mounted under the crystal holder. The space between electronic components and container was filled with epoxy resin to prevent possible degassing.

Since only two terminals are available to connect the oscillator unit to the power supply and frequency counter, the R.F. output is superimposed on the D.C. power supply line by combining a low pass filter and isolation transformer, as is shown in Figure 2.3. Although the emitter follower circuit serves as a buffer stage, the stray capacitance between emitter and base cause slight coupling between load and oscillator. In order to eliminate a possible mismatch at the electronic counter input, the terminal is matched by adding in parallel an additional 50 ohm carbon resister. The characteristic impedance of the coaxial line connecting the isolation transformer and counter is 50 ohms.

An output of 500 mv (r.m.s.) with an 8.2 MHz crystal was obtained across the 50 ohm termination. A 12 volts D.C. supply was used with the R.F. output monitored by a Hewlett Packard 5245l electronic counter. The frequency drift due to the circuit itself is approximately 0.1 hertz per 10 seconds after a 20 minute warmup.

Calibration of Quartz Crystal Microbalance

Although a theoretical calibration (the relationship between the frequency shift of the quartz crystal and the mass

deposited on substrate) is feasible, there are several difficulties involved in such a calibration.

(1) Determination of the exact area and location of the film deposited on the quartz crystal surface.

(2) The relationship between the mass deposited on the quartz crystal and that on the substrate.

An experimental technique was therefore used to determine the constant, c, according to the following procedure.

(1) A mica substrate, the surface area of which is $1.5 \times 3\ cm^2$, is weighed using a chemical microbalance (accuracy of $\pm 2 \times 10^{-6}$ gm).

(2) The change of crystal frequency is measured while the film is deposited on the substrate.

(3) The mass, Δm, deposited on the substrate is determined by reweighing and substracting it from the value obtained in (1).

The constant, c, is given by

$$c = \Delta m/(1.5 \times 3 \times \Delta f).$$

The average value of c for the arrangement shown in Figure 2.1 is given by

$$c = 2.3 \times 10^{-6}\ (gm/cm^2\ hertz).$$

The results obtained for the constant, c, are given below, and the graph is presented in Figure 2.3.

The mass deposited in unit area (gm/cm^2)	17.6	31.3	48.6	72.8
The change of resonant frequency (hertz)	415	731	1098	1672
Value of c	2.36	2.34	2.26	2.30

This value of c corresopnds to 2.41 hertz per Angstrom. The resolution of this microbalance is better than 1 Å for silver films.

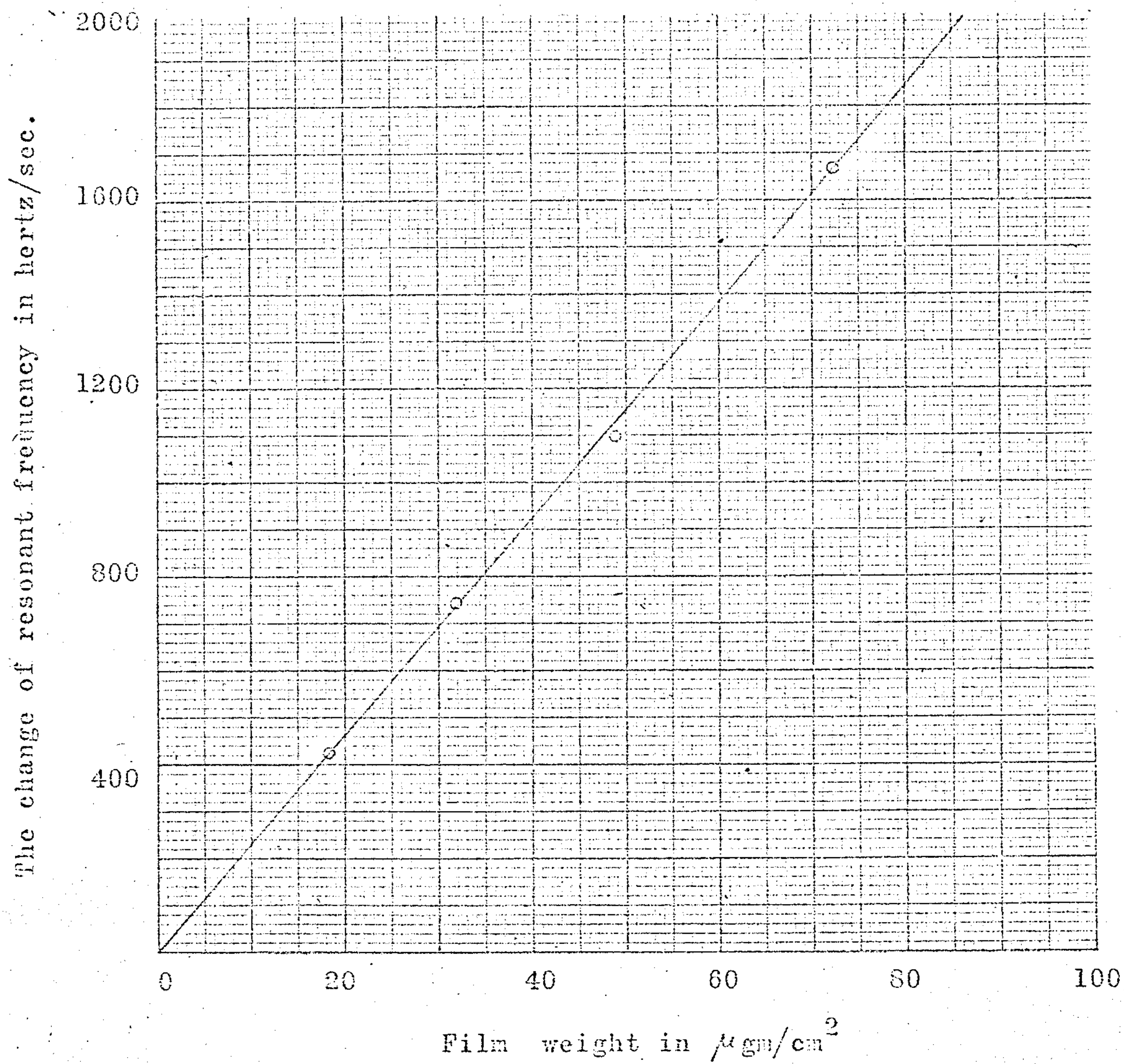

Fig. 2.3 Calibration curve for quartz crystal microbalance.

CHAPTER III

MICROWAVE PROPERTIES OF THIN METALLIC FILM

In this chapter the transmission, reflection, and absorption coefficients of a thin metallic film located in the cross sectional plane of a rectangular waveguide and operating in the TE_{10} mode is analytically determined using the impedance method. The conductivity of a thin metallic film is considered in order to relate the above coefficients to the film thickness.

3.1 Waves in a Conducting Medium

For a rectangular waveguide operating in TE_{10} mode, as shown in Figure 3.1, the propagation constant, γ_{10}, and transverse wave impedance, Z_{10}, in a lossless medium are given by Plonsey and Collin[15] as follow:

$$\gamma_{10} = \sqrt{(\pi/a)^2 - \omega^2\mu\epsilon} \,, \tag{3.1}$$

$$Z_{10} = \omega\mu / \sqrt{\omega^2\mu\epsilon - (\pi/a)^2} \,, \tag{3.2}$$

where a is the waveguide width and ϵ, μ, and ω are permittivity permeability, and angular frequency respectively.

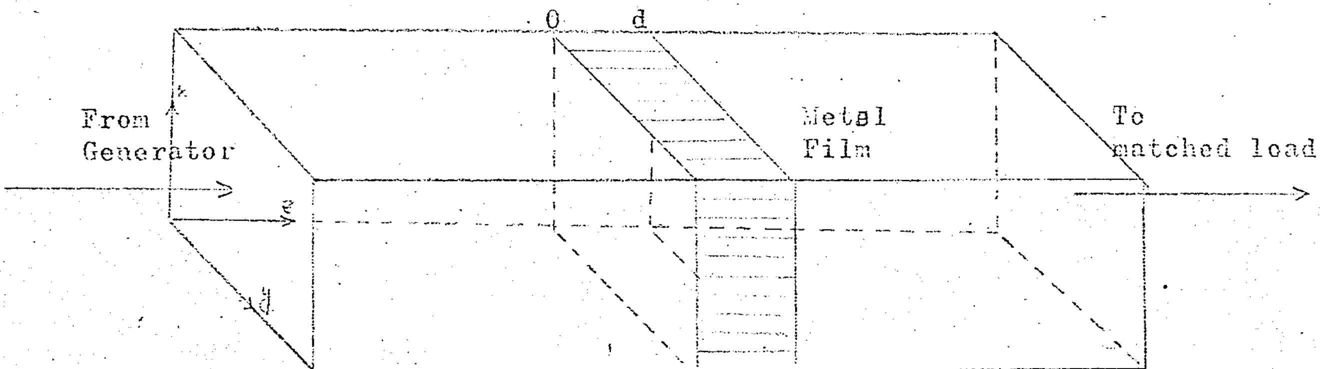

Fig. 3.1 Rectangular waveguede with metallic film

For a conducting medium the curl of the magnetic field expressed in phasor form is

$$\nabla \times \vec{H} = j\omega\epsilon_m \vec{E} \qquad (3.3)$$

where $\epsilon_m = (1 + \sigma/j\omega\epsilon)$ (3.4)

and σ is the specific conductivity of conducting medium.
The propagation constant, γ'_{10}, and transverse wave impedance, Z'_{10}, in a conducting medium in the rectangular wave guide operating in the TE_{10} may be obtained by substituting ϵ_m in place of ϵ in (3.1) and (3.2).
Thus

$$\gamma'_{10} = \sqrt{(\pi/a)^2 - \omega^2\mu\epsilon(1 + \sigma/j\omega\epsilon)}\ , \qquad (3.5)$$

$$Z'_{10} = \sqrt{\frac{\omega^2\mu^2}{\omega^2\mu\epsilon(1 + \sigma/j\omega\epsilon) - (\pi/a)^2}}\ . \qquad (3.6)$$

For a good conducting material the following approximation is valid at microwave frequencies

$$\sigma/\omega\epsilon \gg 1. \qquad (3.7)$$

Using (3.7) equations (3.5) and (3.6) may be now written as

$$\gamma'_{10} = \frac{(1 + j)}{\delta}\ , \qquad (3.8)$$

$$Z'_{10} = \frac{(1 + j)}{\sigma\delta}\ . \qquad (3.9)$$

where is the skin depth defined by

$$\delta = \sqrt{2/\omega\mu\sigma}\,. \tag{3.10}$$

3.2 Thin Film Transmission, Reflection, and Absorption Coefficients.

Identifying the transmitted, reflected, and incident electric field components by the addition of subscripts t, r, and i then the following equations hold at crossection AA' of Figure 3.2.

$$E_i = Z_{10}H_i, \tag{3.11a}$$

$$E_r = -Z_{10}H_r, \tag{3.11b}$$

$$E_t = Z_iH_t \tag{3.11c}$$

where Z_i is the impedance looking to the right of AA'.

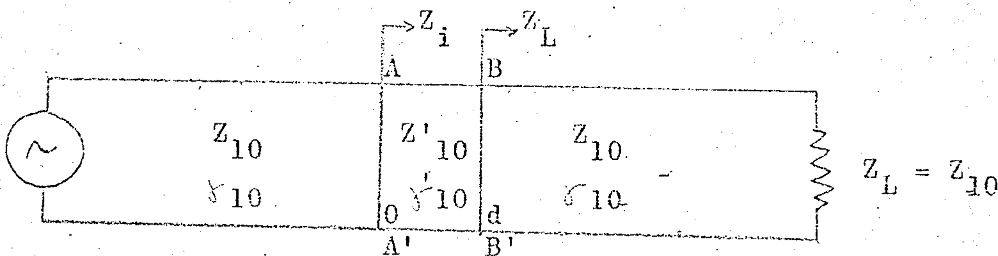

Fig. 3.2 Thin metallic film equivalent circuit.

Equation (3.11) must satisfy the following boundary conditions at AA':

$$E_t - (E_i + E_r) = 0\,, \tag{3.12a}$$

and $$H_t - (H_i + H_r) = E_t/Z_i . \qquad (3.12b)$$

From (3.11) and (3.12) the transmission coefficient, T, and reflection coefficient, R, at AA' can be expressed as follows[15]

$$T = \frac{2Z_i}{(Z_{10} + Z_i)} , \qquad (3.13)$$

$$R = \frac{Z_i - Z_{10}}{Z_{10} + Z_i} . \qquad (3.14)$$

The impedance Z_i at AA' may be obtained by transforming the load impedance Z_{10} at BB' through the metal film[16]. Thus

$$Z_i = Z'_{10} \frac{(Z_{10}/Z'_{10}) \cosh\gamma'_{10}d + \sinh\gamma'_{10}d}{\cosh\gamma'_{10}d + (Z_{10}/Z'_{10}) \sinh\gamma'_{10}d} . \qquad (3.15)$$

Substituting (3.15) into (3.13) and (3.14) one obtains

$$T = \frac{2Z_{10}(Z_{10}/Z'_{10}) \cosh\gamma'_{10}d + \sinh\gamma'_{10}d}{2Z\ (\cosh\gamma'_{10}d + (Z_{10}/Z'_{10})\sinh\gamma'_{10}d) + Z_{10}(Z_{10}/Z'_{10})\cosh\gamma'_{10}d} ,$$

$$\ldots\ldots\ldots\ldots \qquad (3.16)$$

$$R = \frac{Z'_{10}(1 - (Z_{10}/Z'_{10})^2) \sinh\gamma'_{10}d}{2Z_{10}(\cosh\gamma'_{10}d + Z'_{10}(1 + (Z_{10}/Z'_{10})^2)\sinh\gamma'_{10}d} , \qquad (3.17)$$

The following approximation can be made from (3.16) and (3.17). Since Z_{10} is much larger than Z'_{10} for a good conductor, we have

$$T \cong \frac{(1+j)\, k_{10}\cos\theta \cosh \Gamma_{10} d}{\sinh(1+j)(k_{10}\cos\theta + d/\delta)}, \tag{3.18}$$

$$R \cong \frac{-1}{1 + (1+j)\, k_{10}\cos\theta \coth(1+j)d/\delta}, \tag{3.19}$$

where $\cos\theta = \lambda_g/2a$ and λ_g is a guide wave length.

One can make a further approximation from (3.18) and (3.19) for films which are much thinner than a skin depth, $d \ll \delta$, thus

$$T = \frac{1}{1 + Z_{10}\sigma d/2} \tag{3.20}$$

$$R = \frac{1}{1 + 2/Z_{10}\sigma d} \tag{3.21}$$

The absorption coefficient, A, the ratio of absorbed electric field amplitude to incident field amplitude, may be obtained in terms of R and T using the principle of energy conservation. Hence

$$A = \sqrt{1 - R^2 - T^2}\ . \tag{3.22}$$

Substituting (3.20) and (3.21) into (3.22), one arrives at

$$A = \frac{\sqrt{2}}{\sqrt{Z_{10}\sigma d/2} + \sqrt{2/Z_{10}\sigma d}} \tag{3.23}$$

From (3.20), (3.21), and (3.23) we see that the transmission, reflection, and absorption coefficients are a function of the metal conductivity. For a bulk metal, σ is independent of the geometry and the size of material. For a thin film, however, σ is a function of the film thickness. Kaplan[1] gives the following approximations:

$$\sigma(d) = \sigma_o(1 - \Lambda_o/4d), \qquad \text{for } d > \Lambda_o \qquad (3.24a)$$

$$\sigma(d) = \sigma_o(3/4 + 1/2 \ln(\Lambda_o/d)), \qquad \text{for } d < \Lambda_o \qquad (3.24b)$$

where σ_o is the mean free path of a electron in the bulk material and Λ_o is the specific conductivity of the maral in an infinitely thick layer.

The power transmitted, reflected and absorbed in thin silver and gold films is shown in, respectively, Figures (3.3) and (3.4). These curves are obtained from (3.20), (3.21), and (3.23) using the following values of σ_o and Λ_o.

	σ_o in mho/m	Λ_o in Å
Silver	6.139×10^7	570
Gold	4.37×10^7	410

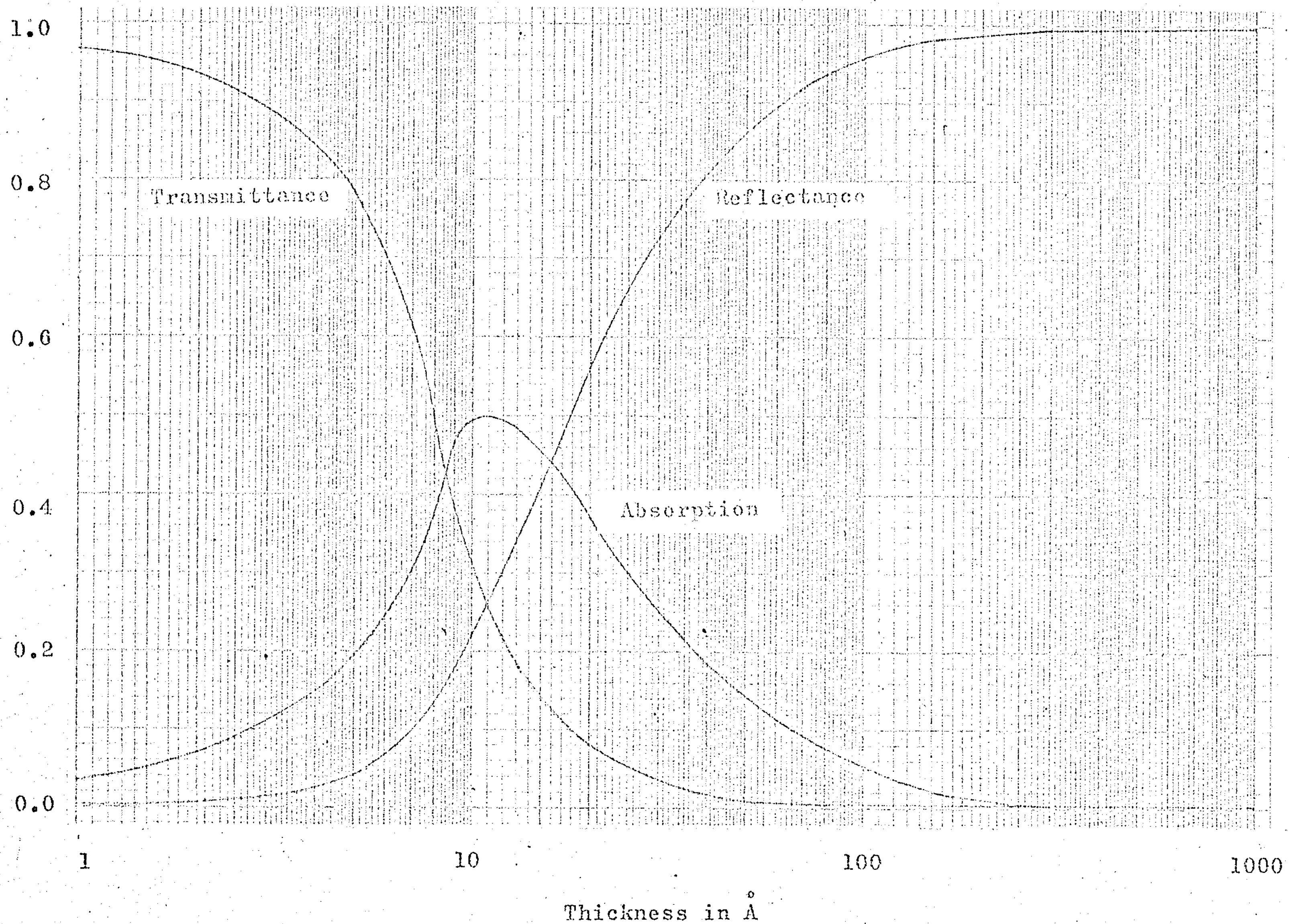

Fig. 3.3 Theoretical transmittance, reflectance, and absorption versus thickness for silver film.

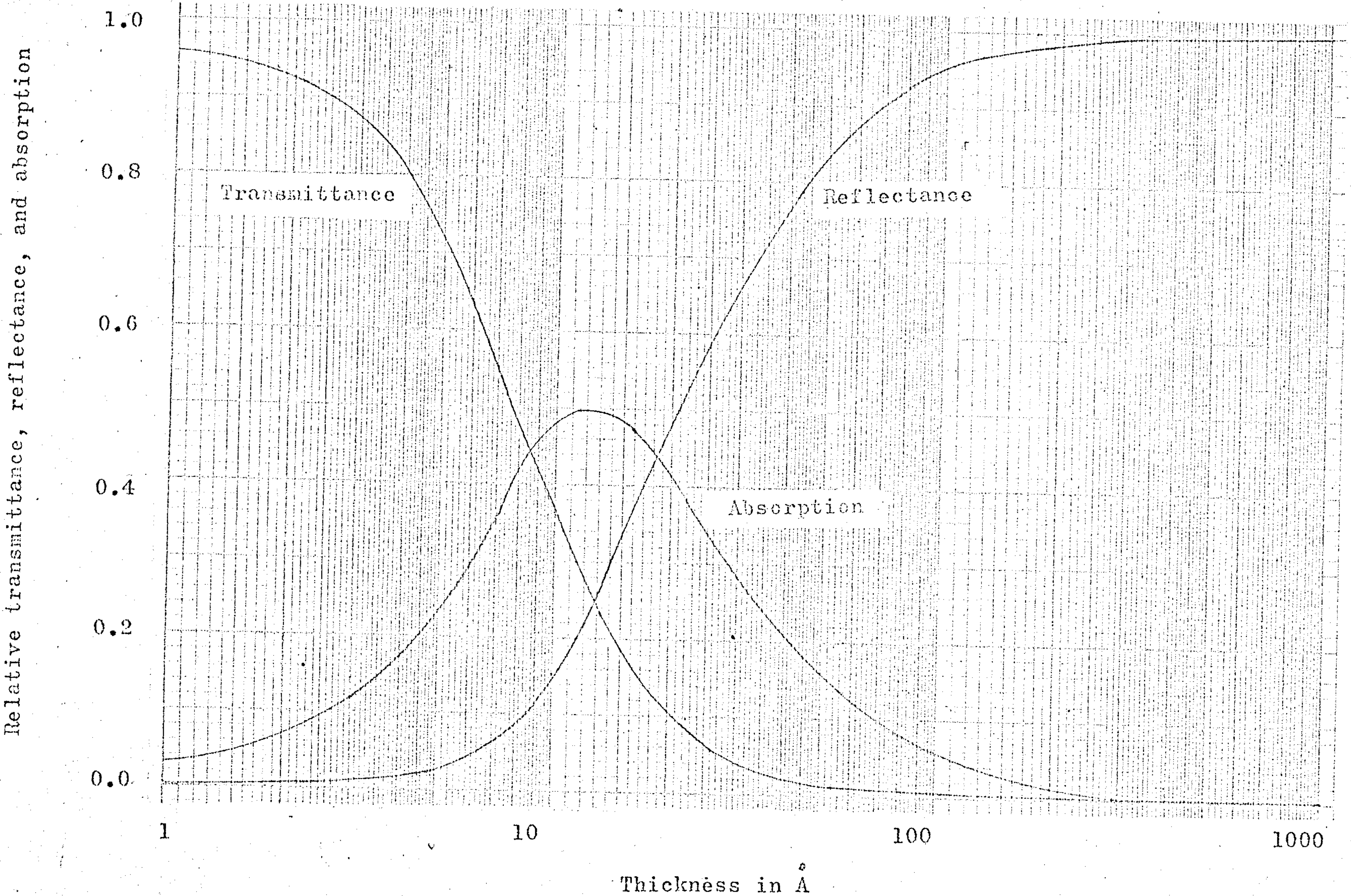

Fig. 3.4 Theoretical transmittance, reflectance, and absorption versus thickness for gold film.

CHAPTER IV

TRANSMISSION COEFFICIENT MEASUREMENT

Although the transmission coefficient, T, can be measured directly against film thickness, d, the experiments were performed in two steps in order to check the results more rigorously. First, film conductivity is examined for various film thicknesses, and secondly, the transmission coefficient is measured versus its conductance per square.

The four probe technique to measure the film conductivity and microwave bridge for transmission coefficient measurement are described in this chapter.

4.1 Thin Film Conductivity Measurement

Generally the conductivity of a thin metallic film is determined by measuring current and voltage across a strip of the film. Since the resistivity of the conducting film is small the contact resistance between the electrode and the film may cause a considerable error. To eliminate this error, the Fell's four probe resistivity measuring device was used. This technique has been analysed by Valdes[17] to measure the conductivity of bulk semiconductor germanum and is modified here to deal with a thin metallic film.

Four Probe Technique

In the four probe technique four collinear, equally spaced probes are placed on the sample surface as is shown in Figure 4.1.

The current flowing through the outer probe set is measured with a milliammeter and the potential difference between the inner probes, B and C, is measured with a potentiometer.

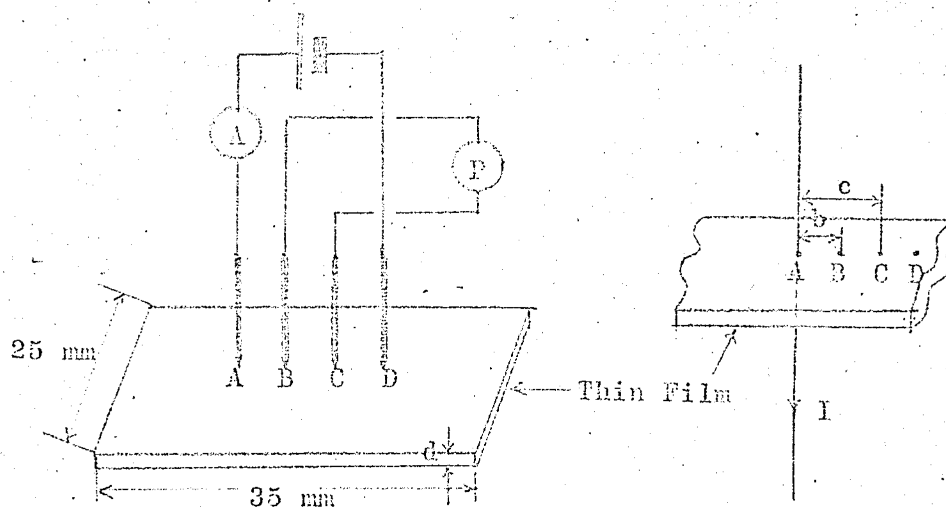

Fig. 4.1 Four probe arrangement

The problem of theoretically determining the potential difference between the inner probes due to the current flowing in the outer probes can be treated as a two dimensional problem since the thickness of the specimen is so much less than the spacing between the electrodes.

Let the potential difference between probes B and C due to the current line source carrying current I be V. Applying Gauss's theorem in cylindrical coordinate one obtains

$$V = (q/2\pi\epsilon)\ \ln(c/b), \qquad (4.1)$$

where q is the charge density per unit length and ϵ is the permitivity of the specimen. Dimensions b and c are the distance of the probes B and C respectively from probe A. The charge

density q can be shown to be

$$q = (2\epsilon/\sigma d)\, I \qquad (4.2)$$

where σ and d are respectively the conductivity and the thickness of the film. Substituting (4.2) into (4.1) one arrives at

$$\sigma = (I/Vd\pi)\ \ln 2, \quad (\text{since } b/c = 2) \qquad (4.3)$$

The Effects Due to the Sample Boundary

Equation (4.3) is derived based on the assumption that the film extends infinitely. Consider the case of the film having two boundaries parallel to the probe array and infinitely extended in the other direction as is shown in Figure 4.2. The potentials at B and C have to be modified due to the electrical images created by the two boundaries. Although those images must decay exponentially according to the reflection coefficient at the boundary, one can make the assumption, without loss of generality, that the magnitude of the images are the same as actual line sources since the film has a high conductivity.

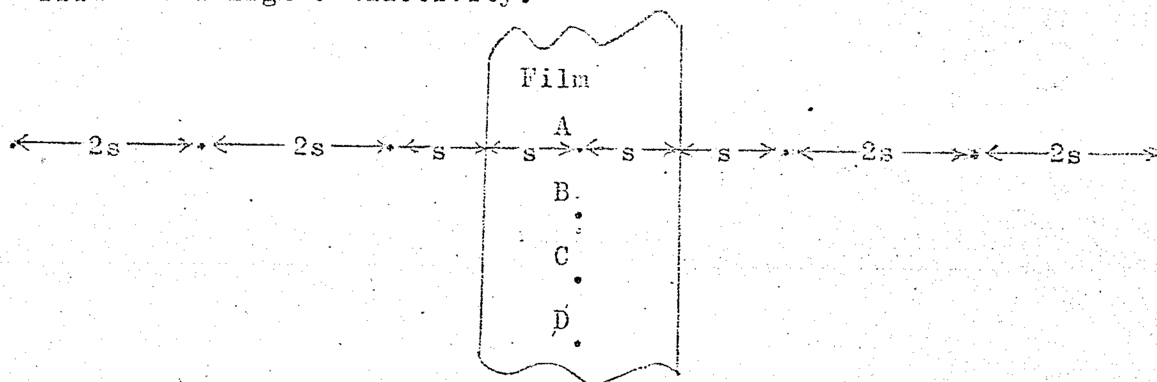

Fig. 4.2 Image due to the film boundary.

The potential at B and C can be expressed in terms of an infinite sum of individual image line sources as shown in Figure 4.2. The final form for the conductivity is obtained by substituting effective values of b' and c' for b and c in (4.3). They are given by

$$b' = \sum_{n=0}^{\infty} \sqrt{(2m)^2 + (2ns)^2} \qquad (4.4)$$

$$c' = \sum_{n=0}^{\infty} \sqrt{m^2 + (2ns)^2} \qquad (4.5)$$

where n is an integer number and s is the distance between the electrodes and boundary. The distance between electrodes is denoted as m. Using (4.3), and (4.4) and (4.5) the conductivity σ is given be

$$\sigma = \sum_{n=0}^{\infty} (I/Vd)(\ln \sqrt{(2m)^2 + (2ns)^2} - \ln \sqrt{m^2 + (2ns)^2}). \qquad \ldots\ldots\ldots\ldots\ldots\ldots(4.6)$$

The first fifty terms in (4.6) were summed using values of 5 mm and 1 mm for s and m respectively. The result turns out to have less than a 3 percent discrepancy from that obtained with (4.3). Hence, (4.3) was used to determine the conductivity without modification.

The conductivity of the thin films was measured using the four probe technique and the values compared to the theoretical values as calculated from (3.24).are shown in

Figure 4.3. The results obtained are given in below.

Thickness in Å	130	220	280	340	560	640	1000
Voltage in mv	0.55	0.23	0.32	0.24	0.16	0.20	0.26
Current in ma	0.60	0.60	1.31	1.31	1.91	2.72	6.0
Conduct.x10^7 in mho/m	1.85	2.60	3.24	3.63	4.70	4.70	5.0

The currents used were such that they were not too high to produce an appreciable heating affect and not too low to affect the sensitivity of the potentiometer.

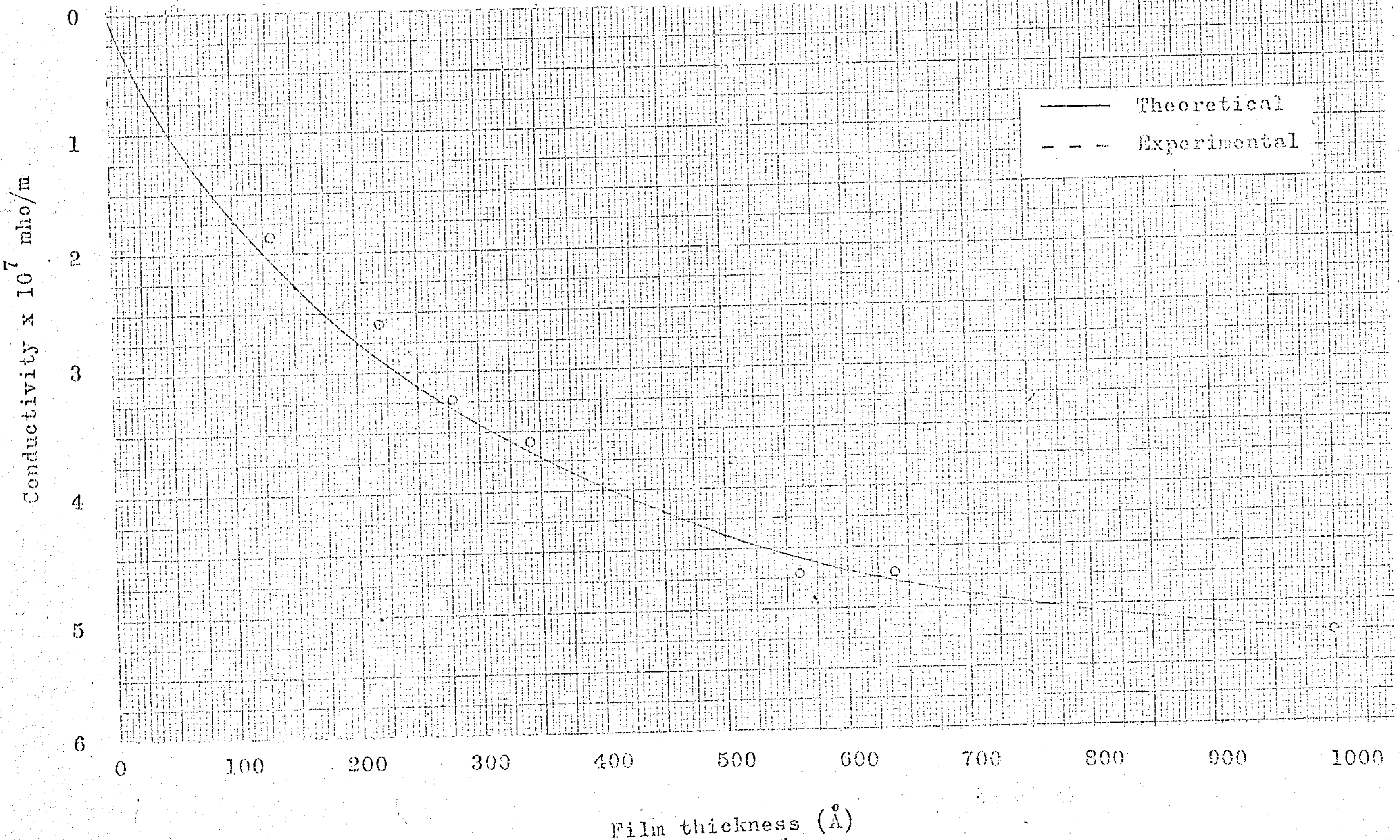

Fig. 4.3 Conductivity versus thickness.

4.2 Transmission Coefficient Measurement

The transmission coefficient of an unknown object inside an X-band waveguide is generally determined by either a substitution or a microwave bridge method. In the substitution method, the output level is kept constant at the detector with and without the unknown object in the circuit by adjusting a calibrated standard attenuator which is connected in series with the unknown object. In this investigation the bridge method was used and it can be explained by referring to Figure 4.4. The reference path, which is composed of a standard attenuator and phase shifter, provides an adjustable level in the range from 0-100 db. Power is split between the reference path and the signal path containing the unknown object. The reference path is adjusted for the same magnitude as the signal path but 180 degrees out of phase with it. The summing of the two signals results in a null reading at the detector. When the unknown object is removed from the signal path, the attenuator in the reference path must be adjusted again to give a null reading at the detector.

In both measurement methods, the attenuation due to the unknown object is given by the difference between the initial (before insertion of the film) and final (after film insertion) settings of the attenuator. The description of the microwave bridge is contained in the following section.

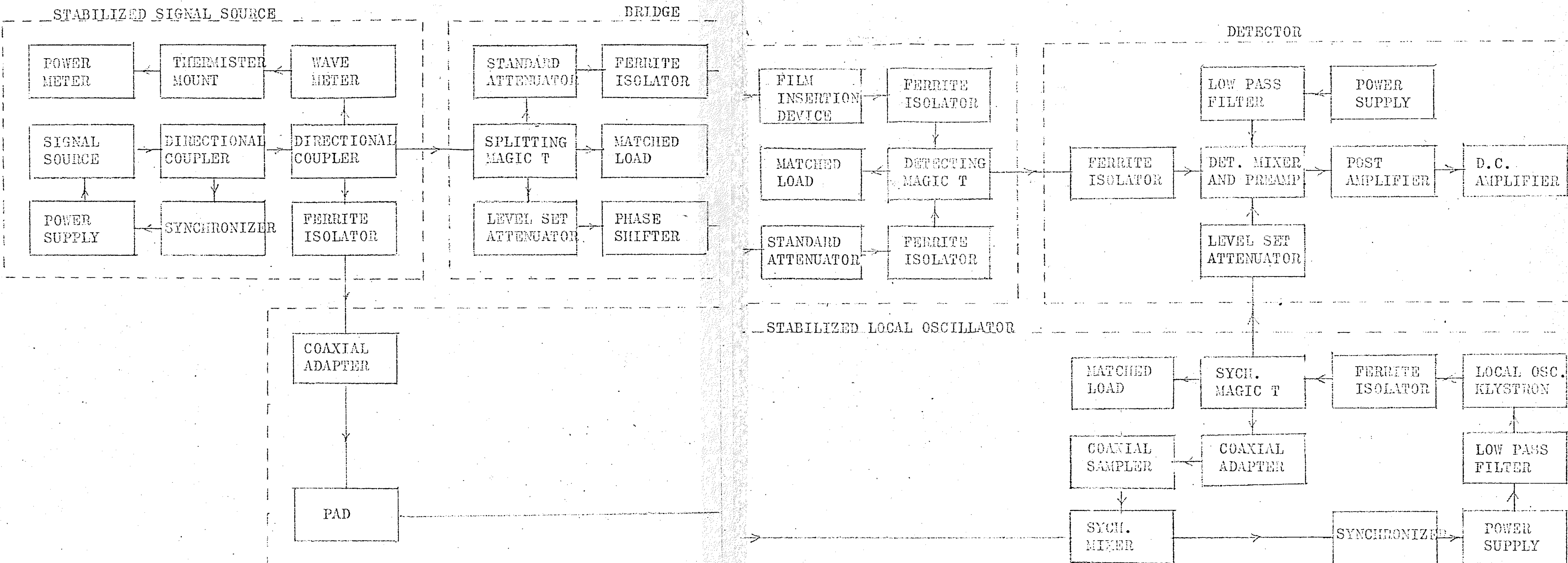

Fig. 4.4 Microwave bredge

Description of Microwave Bridge

The X-band waveguide bridge systems is shown in Figure 4.4 A reflex klystron (X-13) serves as the signal source with a phase locking frequency synchronizer to maintain a constant frequency. The isolation property between H-plane arms of the power splitting magic T is utilized to divide the microwave power coming from the H-plane T junction into the signal and reference paths without coupling them. The signal path consists of a precision rotary attenuator, a ferrite isolator, a film insertion device, and ferrite isolator. The reference path consists of a level set attenuator, a precision rotary attenuator, a precision rotary phase shifter, and ferrite isolator. The two paths are connected at the H-plane junction of a detecting magic T. If signal and reference paths have the same magnitude but opposite phase, the sum of their power is dissipated in the matched load of the E-plane T junction of the detecting magic T, while the output of the H-plane T junction will be zero. In order to detect the null accurately a super-heterodyne detecting system is employed. The detector consists of a synchronized local oscillator, a balanced waveguide mixer, and a 30 Mhz receiver. Although the detecting magic T is designed to provide isolation between H-plane arms, there is, however, a slight coupling (18.8 db). This coupling produces a standing wave between the unknown object and the detecting magic T. As a result, the standing wave may cause a wrong balance condition. In order to provide further isolation between signal and reference paths,

ferrite isolators, connected at the end of reference and signal paths, are employed. Another isolator is also used between the H-plane T and the detecting mixer to prevent interference from the local oscillator.

Frequency Stabilization

High frequency stability of the source klystron is required in order to detect the accurate null condition of the bridge. Any frequency drift in the source causes phase drift at the detecting magic T because of the different electrical path lengths through the two arms. The synchronization of the source klystron is obtained as shown in Figure 4.5. The output of the source klystron is sampled by a 20 db directional coupler and mixed with an R.F. reference output produced by a harmonic generator. The 20 MHz I.F. output of the mixer is amplified and is fed to a discriminator after passing through a limiter stage. The frequency drift in the source klystron is converted to an analog D.C. output in the discriminator by comparing it with 20 MHz I.F. reference signal. This analog output is fed back to the reflector of the source klystron through a video amplifier to compensate for the frequency drift.

Any frequency drift in the local oscillator causes a fluctuation at the output of the 30 MHz I.F. amplifier because of its limited bandwidth. The frequency of the local oscillator must track the frequency of the source klystron so that the intermediate difference frequency output of the detecting mixer remains at 30 MHz. This is accomplished in a manner similar to

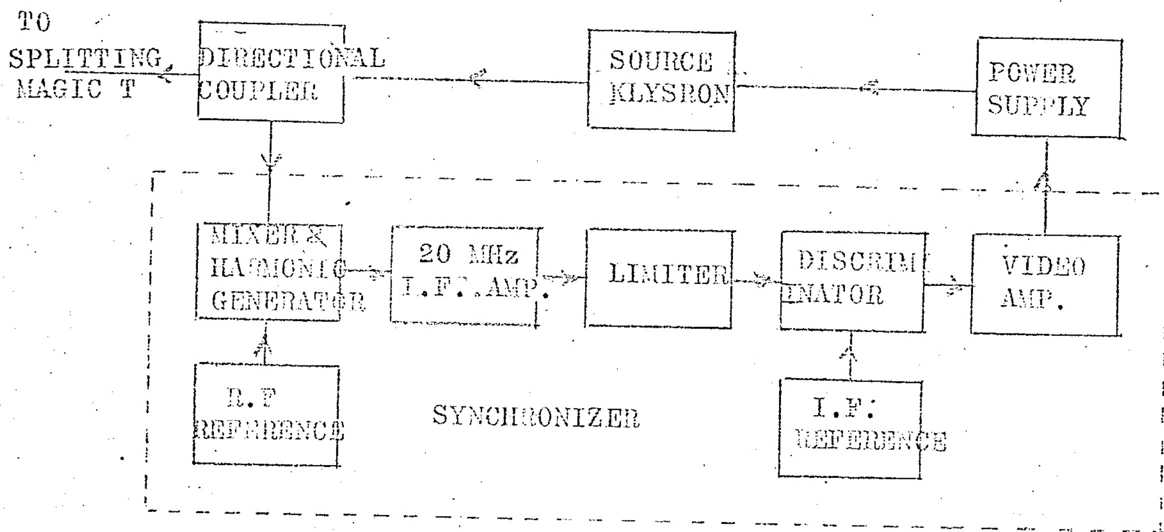

Fig. 4.5 Frequency stabilization of signal source

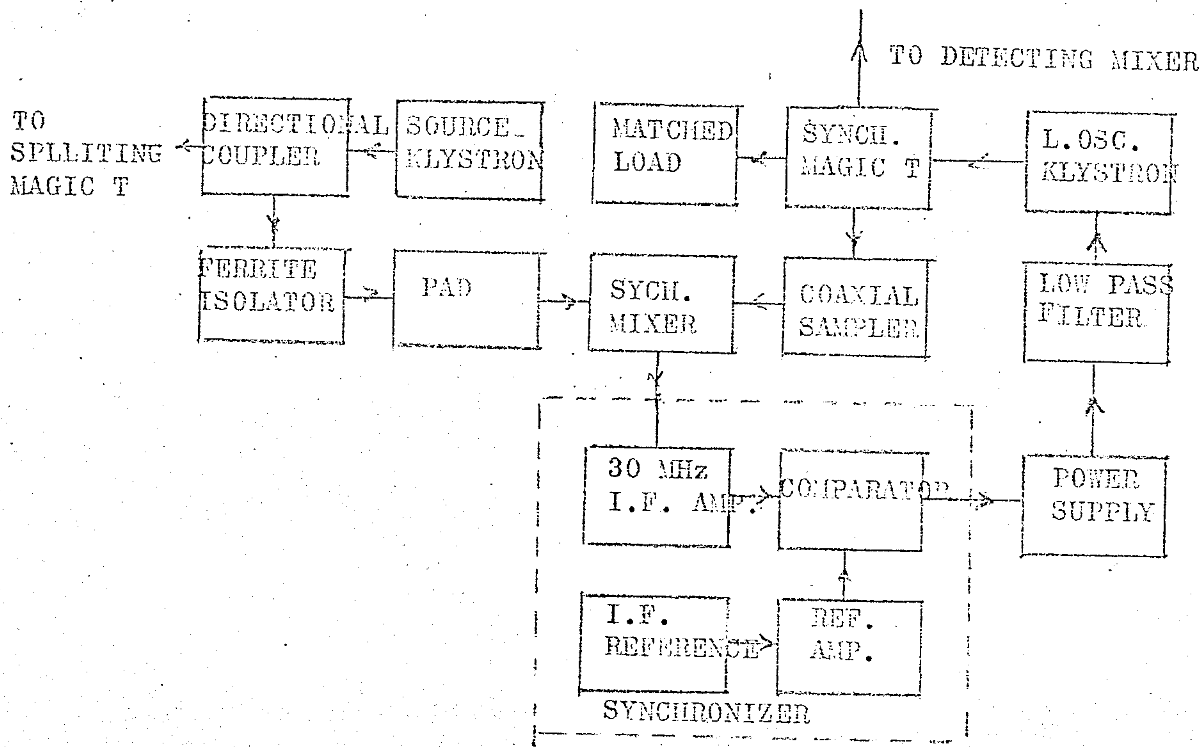

Fig. 4.6 Frequency stabilization of local oscillator

the way the source klystron is locked by using a synchronizng mixer as shown in Figure 4.6.

Certain care must be taken to isolate the receiver and phase control system of the local oscillator synchronizer since they both operate at the same frequency. It was observed that the 30 MHz I.F. reference signal from the discriminator modulated the reflector of the local oscillator and increased the background noise level at the receiver output. A notch filter was inserted between the synchronizer and the reflector of the local oscillator to reject the 30 MHz interfering component without disturbing the phase control network. A two section π network, acting as a low pass filter, was also inserted between the local oscillator and power supply. This filter is shown in Figure 4.7. Another similar filter was placed between the 30 MHz preamplifier in the receiver and its power supply.

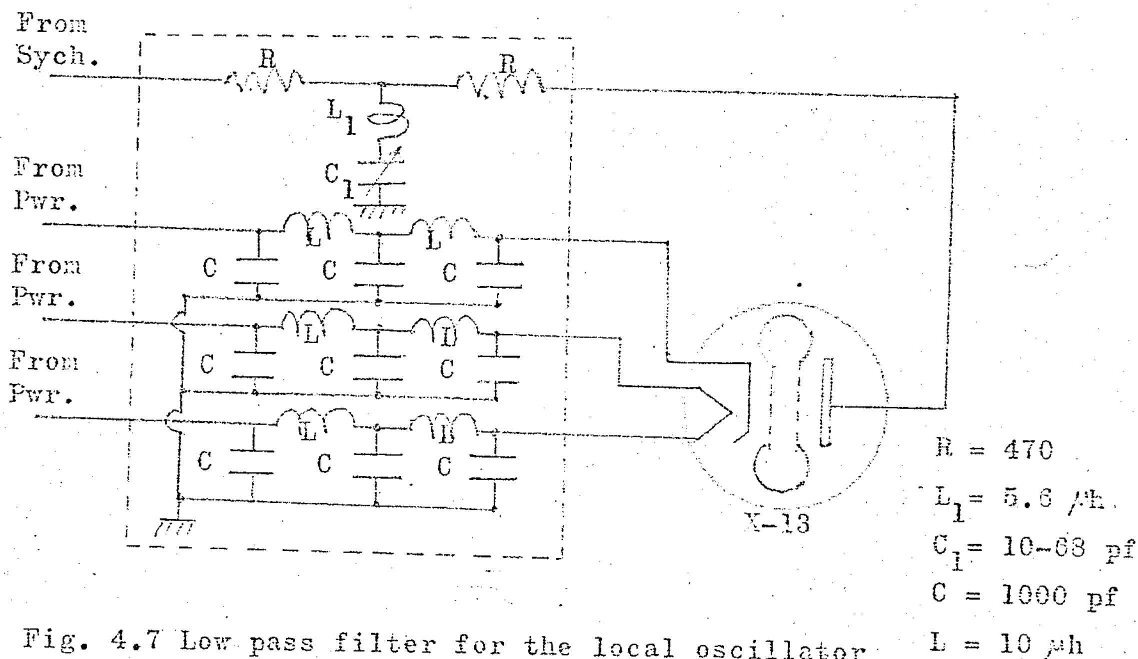

Fig. 4.7 Low pass filter for the local oscillator

A 10 GHz leakage through the synchronizing mixer to the local oscillator channel caused serious interference. The isolation characteristic between an H-plane T junction and an E-plane T junction of a magic T was utilized to prevent the 10 GHz leakage. A ferrite isolator and a 30 db coaxial pad were used to further reduce the undesired coupling. The input signal of the synchronizing mixer was maintained at as small a level as possible with a coaxial sampler for further isolation. The overall suppression was approximately 140 db. The frequency drift in the source klystron was of the order of 20 parts in 10^{10} and the frequency drift between the local oscillator and the source negligible.

Film Insertion Device

It was found necessary to develop a technique to insert the film into the waveguide without disturbing the mechanical connections of the bridge. This was necessary in order to preserve the accurate initial balance condition. A modified shorting switch (Hewlett Packard Model X-930) was used as a means of placing the film in the waveguide. A metal slider was built which would fit the shorting switch slot and which could slide the plate into the waveguide in a manner shown in Figure 4.8. The film, deposited on the mica substrate, is placed between two metal pieces and inserted into the sliding metal plate.Silver paint was coated on the metal pieces and film edge to provide a good electrical contact. Leakage through the insertion device was very important since the transmittance

of the metallic film is very small. A quarter-wave choke flange was used to minimize the leakage between the metal sliding plate and wave-guide junction. The system was checked by inserting a piece of thick aluminium foil in place of the film and the leakage was consistently found to be 90 db below than the incident level. This amount of leakage may introduce, at worst, one percent error at the maximum attenuation (70 db) used in the measurement of transmittance.

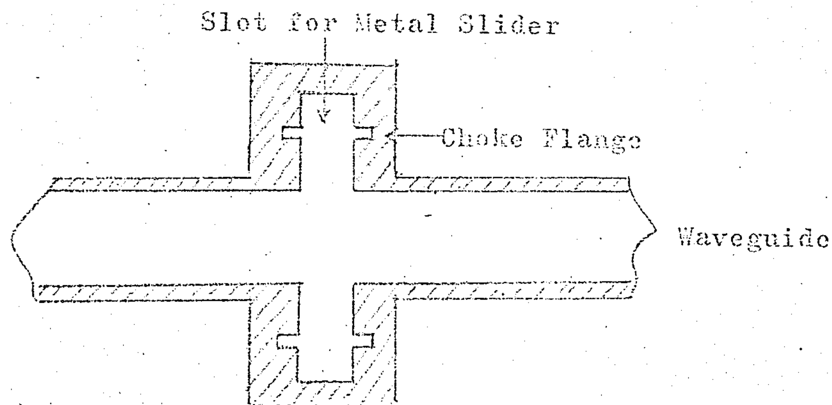

WAVEGUIDE SHORTING SWITCH

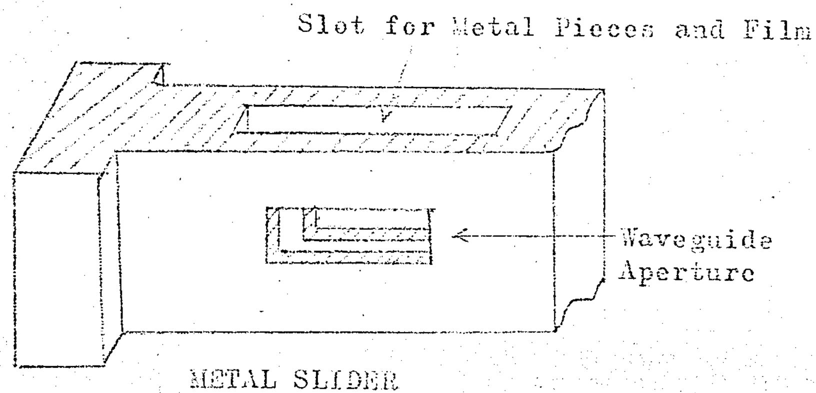

METAL SLIDER

Fig. 4.8 Film insertion device

The transmission coefficient of the silver film was measured using the microwave bridge method and the values obtained were plotted against the conductance per square (σd). Each point obtained in Figure 4.8 was measured from two samples to check the reproducibility of the experimental results.

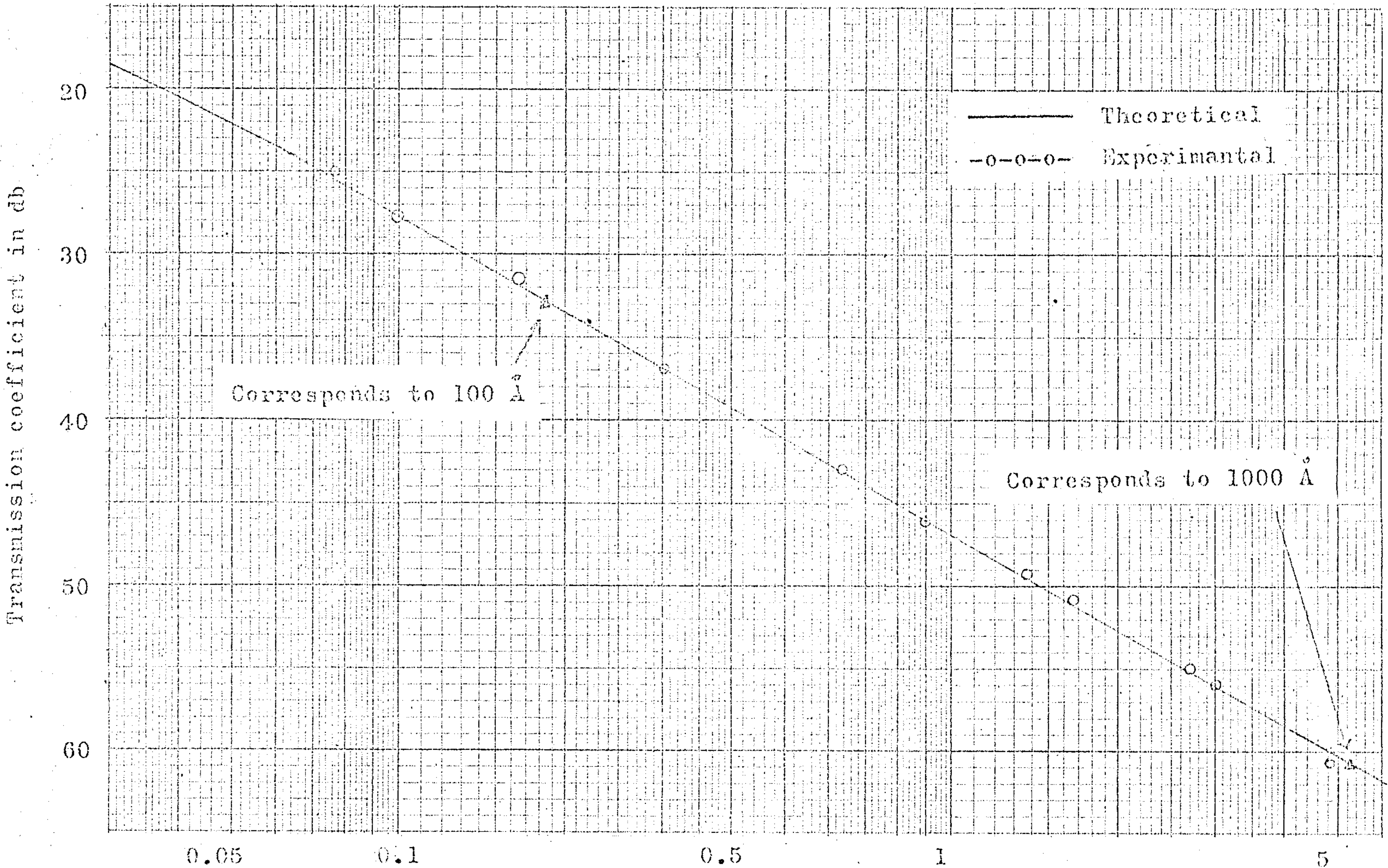

Fig. 4.9 Comparison of experimental and theoretical transmission coefficient versus conductance per square.

CHAPTER V

DISCUSSION AND SUMMARY OF RESULTS

The results of film attenuation versus film thickness are given in Figure 5.1. The curve shows that the measured values of attenuation differ from the theoretical values by at most 1 db. It was observed that the thicker films (greater than 500 Å) all have a slightly higher attenuation than that predicted theoretically. We may attribute this to the imperfect contact of the film with the waveguide wall.

The transmittance formula as given by Kaplan, equation (3.20), is valid for frequencies less than 10^3 GHz. The experimental results of this thesis verify the formula at the microwave frequency of 10 GHz. Weck and Lump performed an experiment[3] in the frequency range 50 KHz to 1 GHz using film thicknesses of 1400 Å and 4500 Å. Their results were in good agreement with theory.

An attempt was made to produce a film of less than 100 Å. However, the results were not consistant and this may possible be due to the granular film structure. It is difficult to obtain experimental attenuation values for films in such a thickness range. An attenuation versus conductance per square curve was found however to agree with the theoretical one as is shown in Figure 4.9.

The four probe technique of measuring conductivity was compared with the conventional method (determined by measuring

current and voltage drop across the films) and they agree within 5 percent for well prepared film. The measurements indicate that it is technically feasible to use a four probe technique for the purpose of determining the local conductivity of thin films provided that the spacing between probes can be made sufficiently small.

An attempt was made to measure the phase shift due to a thin film. It was found that the precision rotary attenuator introduced an unwanted phase shift of as much as 10 degrees in the attenuation range 0-50 db. This problem may be overcome by calibrating the attenuator. The film insertion device itself causes about a 3 degrees phase uncertainty for film thicknesses of 1000 Å (corresponding to an attenuation of 60 db) due to the imperfect electrical contact. A theoretical calculation indicates that a 1000 Å thick film should introduce only 0.38 degrees phase shift. Hence, phase shift could not be measured with any reasonable accuracy.

An attempt was also made to determine the reflection coefficient parameter by measuring the standing wave ratio, SWR. The apparatus used was capable of measuring the SWR up to 40 db, corresponding to a film thickness of about 130 Å. For film thickness less than 100 Å. it was not possible to relate the reflection coefficient to the film thickness owing to the granular structure of the films. However, the reflection coefficient versus conductance per square could be determined

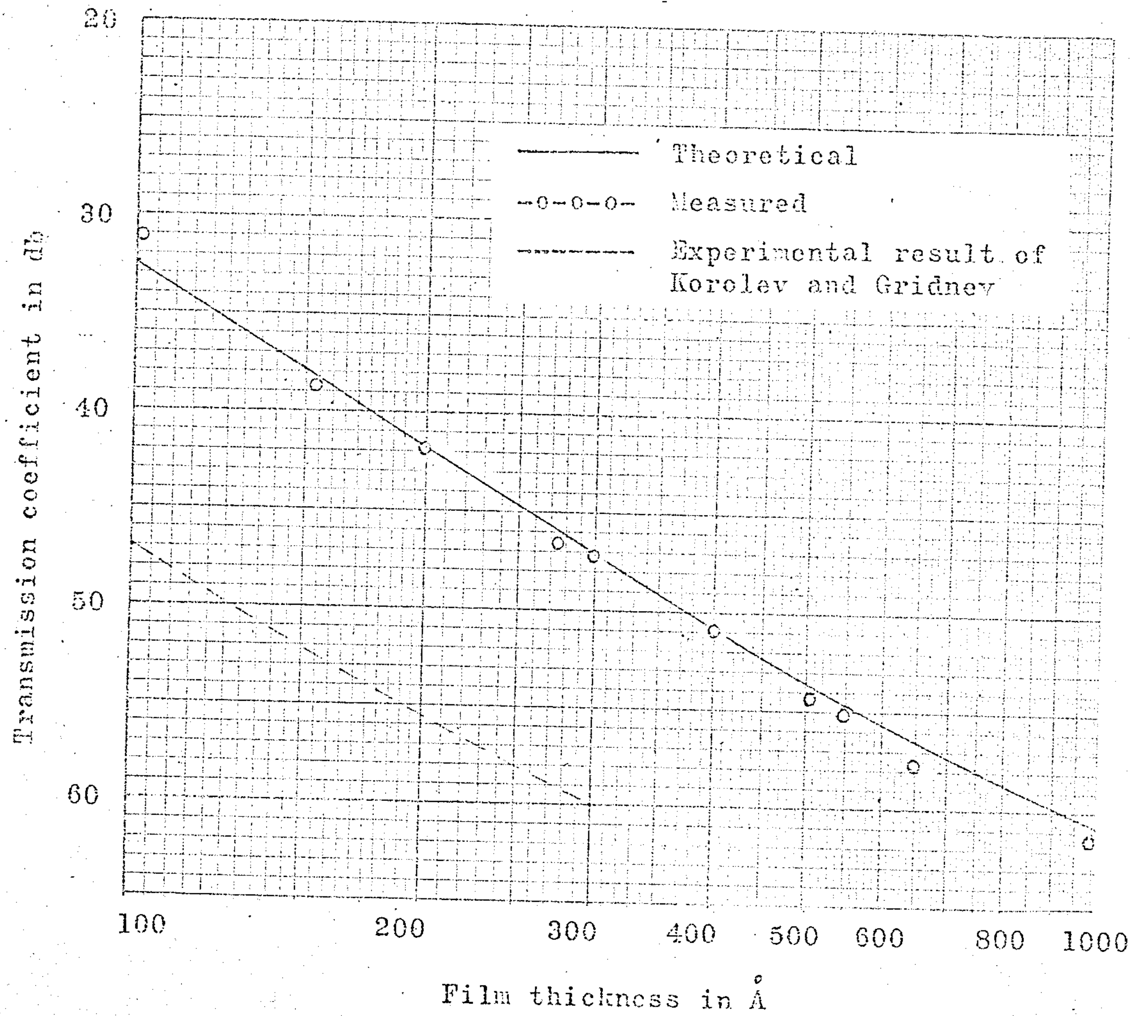

Fig. 5.1 Comparison of experimental and theoretical transmission coefficient versus film thickness for silver.

and the experimental results agreed reasonably well with the theory.

The transmission coefficient measurement of a thin metallic film accurately determines the conductance per square of a given thin conducting material. This measurement can be made over a wide frequency range and eliminates the need for positioning electrodes.

Experiments were also performed using gold films. The gold films were prepared using the same evaporation technique as that for silver, but the conductance per square was measured by the strip method and the thickness determined by a chemical weighing method. The results are summarised in Figure 5.2 and as can be seen the difference between the theoretical and experimental curves is considerable. This is very probable due to the existence of discontinuities in the structure of the gold film as had been reported by many authors[18]. The strip method of measuring the conductance, which actually measures the conductance of the whole strip rather than the local conductance in a small region, also limits the accuracy of results.

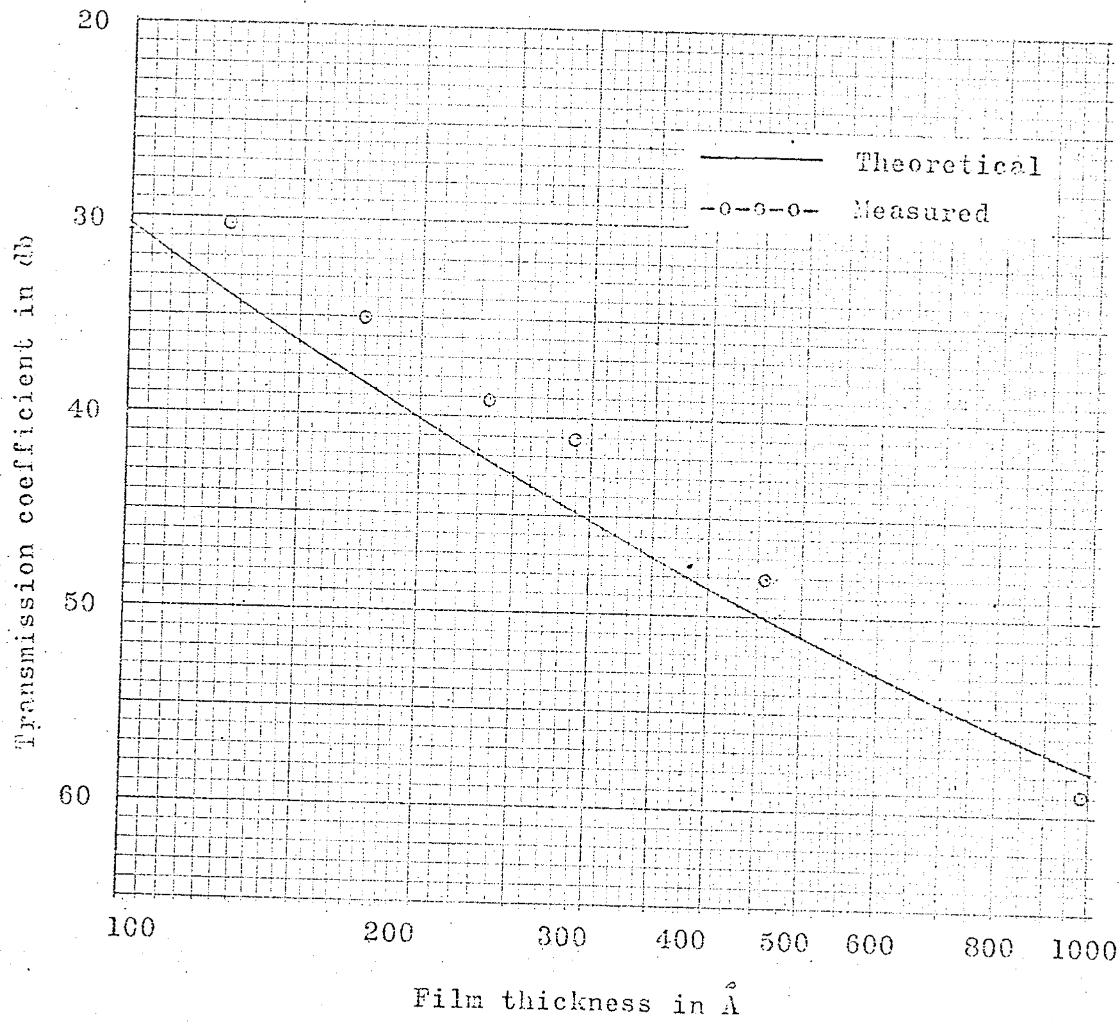

Fig. 5.2 Comparison of experimental and theoretical transmission coefficient versus film thickness for gold.

REFERENCES

1. A.Ye. Kaplan. On the Reflectivity of Metallic Films at Microwave and Radio Frequencies, Radio Engineering and Electronics Phys., Vol. 9, P. 1467; 1964

2. F.A. Kolorev and V.I. Grednev. Transmission of Electromagnetic Waves through Thin Silver Films, Radio Engineering and Electronics Phys. Vol. 10, P. 1476; 1965

3. R.A. Weck and C.J. Lump. Plane-Wave Shielding Effectiveness Studies of Thin Films, Proc. of I.E.E.E., Vol.55, P. 596; 1967

4. A.Ye.Kaplan. On the Brief Communication "Transmission of Electromagnetic Waves Through Thin Silver Films" by Kolorev and Gridnev, Radio Engineering and Electronics Phys., Vol. 11, P. 1677; 1966

5. F.A. Korolev and V.I. Gridnev. Author's Reply to A.Ye. Kaplan's Letter, Radio Engineering and Electronics Phys., Vol. 11, P. 1678; 1966

6. O.S. Heavens. Contamination in Evaporated Films by Material of Source, Proc. Phys. Soc. Vol. 65, P.788; 1952

7. J.M. Ziman. Electrons and Phonons, Claredon Press, P. 335

8. E.J. Lewis. A Survey of the Production and Management of Vacuum Deposited Thin Solid Films, Technical Report 400-46, N.Y. Univ.; 1962

9. E.S.T. Appleyard. Some Factors Influencing the Resistance of Thin Metallic Films, Proc. Phys. Soc. Vol. 49, E.P.118; 1937

10. E.J. Lennard-Jones. The Migration and Aggregation of Atoms on Solid Surfaces, Proc. Soc. A. 121, P. 247; 1928

11. H. Levinstein. The Growth and Structure of Thin Metallic Films, J. of Appl. Phys., Vol. 20, P. 307; 1949

12. F.W. Reynold ang G.R. Stilwell. Mean Free Paths of Electrons in Evaporated Metal Film, Phys. Rev., Vol. 88, P. 201; 1952

13. P.L. Clegg and A.W. Crook. A Torsion Balance for Weighing Evaporated Films, J. Sci. Inst., Vol. 29, P. 201; 1952

14. S. Tolansky. Multiple Beam Interferometry, Calendon Press, 1948

15. G. Saubrey. Application of Vibrating Quartz to the Weighing of Thin Films for Microweighing, Z.f. Phys., Vol. 155, P. 206; 1959

16. Plonsey and Collin. Principles and Applications of Electromagnetic Fields, McGraw-Hill, P. 355; 1961

17. L.B. Valdes. Resistivity Measurement on Germanium for Transistor, I.R.E. Proc. Vol. 43 P. 420; 1954

18. R.S. Sennett and G.D. Scott. The Structure of Evaporated Metal Films and their Optical Properties, J. of Opt. Soc. of Am. Vol. 40, P. 203; 1950

19. O.S. Heavens. Optical Properties of Thin Solid Films, Dover, P. 8; 1954